Electrochimica Acta 531 (2025) 146266

Contents lists available at ScienceDirect

Electrochimica Acta

journal homepage: www.journals.elsevier.com/electrochimica-acta

Semianalytical approximation of Ion Adsorption Layers and Capacitance in Carnahan–Starling-like steric models

Dagmawi B. Tadesse [a], Drew F. Parsons [b,a,*]

[a] School of Engineering and Energy, Murdoch University, 90 South Street, Murdoch, 6150, WA, Australia
[b] Department of Chemical and Geological Sciences and CSGI, University of Cagliari, Cittadella Universitaria, S.S. 554 bivio Sestu, Monserrato, 09042, CA, Italy

ARTICLE INFO

Keywords:
Carnahan–Starling equation
Steric forces
Semianalytical Carnahan–Starling approximations
Electric double layers
Electric double layer capacitors

ABSTRACT

The Carnahan–Starling (CS) steric model is the best description of hard-sphere fluids within the mean-field theory. Here we introduce an approximation of the near-linear adsorption concentration profile of a counterion near an electrode for a CS model and derive the subsequent electric field and electrostatic potential profile in a double layer. This enables the derivation of a semianalytical approximation of the electrode charge density, differential capacitance, and total energies (grand potentials) of an electric double-layer capacitor. These semianalytical equations are valid for electrode potentials between 0.2–4 V and converge to the full numerical solutions of the CS model at high potentials of 1V and bulk concentration of 1M with relative errors less than 2% for the electrode charge densities, and less than 5% for the capacitance and total energies. We find the steric contribution comprises approximately one-quarter of the total energy at high electrode potentials, while the contribution from ideal ion entropies becomes insignificant. The model shows very good agreement with experimental measurements of an aqueous electrolyte, and good agreement at high potentials with computer simulations of an ionic liquid. These semianalytical approximations are effective for applications with concentrated solutions or ionic liquids at high applied voltages where the full numerical solution is computationally expensive or in some cases impossible.

1. Introduction

Supercapacitors, also known as electric double-layer capacitors (EDLC), are a class of energy storage devices with high power characteristics that make them desirable for fast charging and discharging processes, even though their energy density may be lower than redox-type devices (batteries). A supercapacitor operates via the formation of an electric double layer (EDL) when charged electrodes contact an electrolyte solution. The performance of these devices in terms of capacitance and energy density depends on the structure of the EDL. Modelling the EDL structure accurately helps in optimizing the performance of these storage devices. A dilute solution model such as the Poisson–Boltzmann model describes the EDL sufficiently well for low potentials (<0.1 V) and, as the name suggests, for dilute electrolyte solutions. However, in electrochemical systems electrode potentials are typically high (>1 V), and the capacitance of EDLCs is maximized by the use of concentrated electrolytes exceeding 1 mol/L. In these conditions, the dilute solution model breaks down due to neglect of finite ion sizes, resulting in unbounded ion concentrations and capacitance and consequently unphysically high stored energy. A more realistic model can be constructed by incorporating steric forces driven by finite ion sizes. The chemical potential μ_i, of the i^{th} ion, can be written as $\mu_i = \mu_i^{\text{id}} + \mu_i^{\text{ex}}$, where $\mu_i^{\text{id}} = k_{\text{B}}T\ln(\phi_i/\phi_{ib})$ is the ideal (entropic) chemical potential of the ion, k_{B} is Boltzmann constant, T is temperature. $\phi_i = c_i v_i$ is the volume fraction of the ion with size v_i and concentration c_i, while ϕ_{ib} is the reference volume fraction in bulk solution. μ_i^{ex} is the excess chemical potential relative to the reference bulk solution, defined in conventional dilute solution theory solely by the electrostatic potential, $\mu_i^{\text{ex}} = z_i e\boldsymbol{\Phi}$, z_i being the valence number of the i^{th} ion, e the elementary charge, and $\boldsymbol{\Phi}$ the electrostatic potential.

Finite size effects are introduced by adding a steric potential μ_i^{st} to the excess chemical potential. There have been numerous attempts to account for the ion size within mean field theory dating back to Bikerman [1–8]. The simplest model to account for ion size is given by a composite diffuse layer (CDL) [7], where the steric force is activated to maintain a concentration cap determined by ion size [9–11]. The CDL approach can be considered as the asymptotic limit of an excluded volume or solvent entropy model [6,11]. The most common form of the excluded volume model is the Bikerman model [1] with $\mu_i^{\text{bik}} = -k_{\text{B}}T\ln(1-\varphi)$, which conveniently enables a closed-form expression for the Boltzmann concentration profile of ions. Here $\varphi = \sum_i \phi_i$ is the

* Correspondence to: Curtin Institute for Data Science, Curtin University, Kent Street, Bentley, WA 6102, Australia.
E-mail address: drew.parsons@unica.it (D.F. Parsons).

https://doi.org/10.1016/j.electacta.2025.146266
Received 30 December 2024; Received in revised form 25 March 2025; Accepted 17 April 2025
Available online 8 May 2025

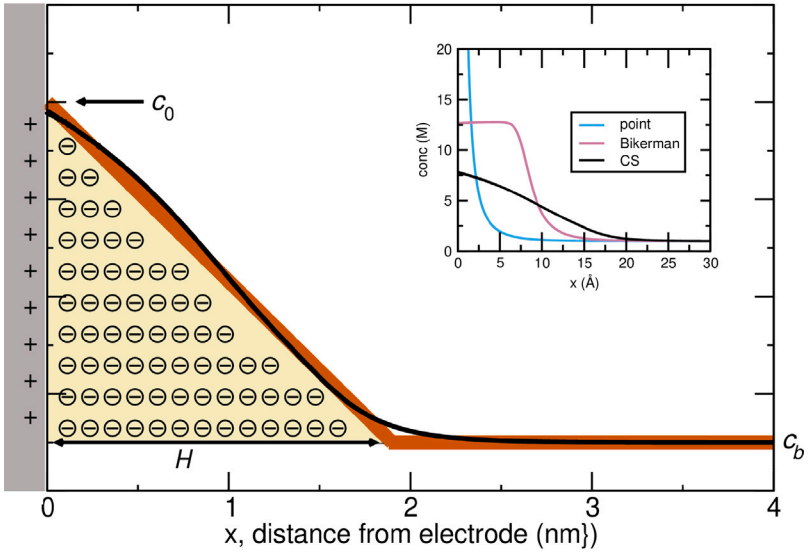

Fig. 1. Diagram of a counterion concentration profile (anions) next to an electrode (positively charged), showing a linear profile (red line) from surface concentration c_0 to bulk concentration c_b at distance H, compared with a Carnahan–Starling profile (black curve). Profiles from Bikerman (capped steric layer) and point charge (exponential) models are shown in the inset for comparison. The illustration uses 1M $LiPF_6$ in propylene carbonate with 1 V electrode potential (relative to bulk solution), PF_6^- as counterion.

total volume fraction of all ions. At high potentials, both the CDL and Bikerman models predict saturation of counterions near the surface of an electrode, forming a steric layer of near-constant concentration. The formation of a fixed steric layer enables the derivation of analytical equations of the surface charge density and differential capacitance of an EDL. These excluded-volume models successfully give insight into the structure of an EDL [7,11,12]. Nevertheless, they continue to overpredict the adsorption concentration of ions and therefore the capacitance [7,8,11–13]. A more accurate description of the steric interaction is provided by Equation-of-State models [14–16], of which the Carnahan–Starling (CS) model [3,17,18] is best known, given by

$$\mu_i^{\mathrm{st:CS}} = k_B T \frac{\varphi(8-9\varphi+3\varphi^2)}{(1-\varphi)^3} \tag{1}$$

The CS model provides an accurate model of the equation of state of a hard-sphere fluid. Despite the accuracy, its highly nonlinear nature makes it difficult to implement. Derivation of analytical equations of the surface charge densities, differential capacitance, and total energies of an EDL is also nearly impossible.

Nevertheless, it is possible to construct semi-analytic expressions describing the electric double layer of the CS model (and other EOS models). This is motivated by the observation [13] that the counterion concentration profile of these models under high electrode potentials is nearly *linear*, distinct from the fixed flat steric layer formed by excluded-volume (Bikerman) models, shown in Fig. 1.

2. Theoretical background

The electrostatic potential is determined by the Poisson equation

$$-\nabla\cdot\varepsilon_0\varepsilon_s\nabla\Phi(x) = \sum_i^N z_i e c_i(x) \tag{2}$$

where ε_0 is the vacuum permittivity, ε_s is the dielectric function of the solvent medium. In thermal equilibrium, the Poisson equation is coupled with the Boltzmann equation that determines concentration profiles

$$c_i(x) = c_{ib}\exp\left(-\beta\Delta\mu_i^{\mathrm{ex}}\right) \tag{3}$$

where $\beta = 1/k_B T$ Using the CS model, the excess chemical potential in Eq. (3) will be $\Delta\mu_i^{\mathrm{ex}} = \mu_i^{\mathrm{el}} + \Delta\mu_i^{\mathrm{st:cs}}$ is the change in the excess chemical potential of the ion from the reference bulk and $\beta = 1/k_B T$. $\Delta\mu_i^{\mathrm{st:cs}} = \mu_i^{\mathrm{st:cs}} - \mu_i^{\mathrm{st:cs,bulk}}$ is the change in the steric potential relative to the bulk reference.

2.1. Semianalytical EDL structure

Full numerical solutions of the CS model show that the concentration profile of counterions follows a roughly linear profile (Fig. 1). Hence at sufficiently high potential and concentration, the counterion concentration can be approximated by

$$c(x) = \frac{c_b - c_0}{H}x + c_0 \tag{4}$$

where c_b and c_0 are the concentration of the counterions in bulk and at the electrode interface, respectively. Here we have dropped index i and refer solely to the counterion, assuming that the coion concentration is negligible under conditions of high potential. The counterion concentration at the interface corresponds to the surface volume fraction φ_0, with $c_0 = \varphi_0/v$, where v is the volume of the counterion. H is the thickness of the steric layer, which will be determined below. The volume fraction in the steric layer then follows $\varphi(x) = vc(x)$. Outside the steric layer, i.e. $x \geq H$, ionic concentration is given by the bulk concentration $c(x) = c_b$. With a linear charge distribution, the electric field (first integral of the Poisson equation) becomes

$$E(x) = \frac{ze(c_b - c_0)}{2\varepsilon H}x^2 + \frac{zec_0}{\varepsilon}x - \frac{ze(c_0 + c_b)}{2\varepsilon}H \tag{5}$$

where $\varepsilon = \varepsilon_0\varepsilon_s$. Here a boundary condition of zero electric field in the bulk has been taken, i.e. $E(x = H) = 0$. If a mean constant value for the dielectric constant ε_s inside the linear steric layer is assumed, then the electric potential $\Phi(x) = -\int E(x)dx$ with the condition that it also goes to zero at bulk, $\Phi(x = H) = 0$,

$$\Phi(x) = -\frac{ze(c_b - c_0)}{6\varepsilon H}x^3 - \frac{zec_0}{2\varepsilon}x^2 + \frac{ze(c_0 + c_b)H}{2\varepsilon}x - \frac{ze(c_0 + 2c_b)H^2}{6\varepsilon} \tag{6}$$

To find an expression for the steric layer thickness H, we use the condition that at the electrode interface the potential is the surface potential $\Phi(x = 0) = \Phi_0$, giving

$$H = \sqrt{-\frac{6\varepsilon\Phi_0}{ze(c_0 + 2c_b)}} \tag{7}$$

The steric layer thickness increases with increasing electrode potential, Φ_0, as one would expect.

3. Semianalytical approximation

The analytical expressions above require the determination of the counterion surface concentration c_0, equivalent to determining the total

ion volume fraction φ_0 at the surface. This is evaluated from the surface potential Φ_0. Recalling that $\varphi = \sum_i c_i v_i$ here (bringing back coions with index i to aid discussion), and noting that concentrations c_i are given by the Boltzmann equation, Eq. (3), we construct an equation [19] relating volume fraction φ to potential Φ,

$$\varphi - \sum_i c_{ib} v_i \exp(-\beta z_i e\Phi)\, \exp(-\beta \Delta\mu^{cs}(\varphi)) = 0 \tag{8}$$

Then, assuming the coions are negligible in the surface adsorption layer, we may estimate the volume fraction at the interface, φ_0 as the root of the equation

$$\varphi_0 - c_b v \exp(-\beta z e \Phi_0) \exp(-\beta \Delta\mu^{cs}(\varphi_0)) = 0 \tag{9}$$

Because of the exponential function and the nature of the steric potential $\mu^{cs}(\varphi)$ as a function of volume fraction φ, this equation is transcendental and the root φ_0 cannot be found analytically. But it is easily evaluated numerically, providing φ_0 (and therefore c_0) as a function of surface potential Φ_0. Taken with the analytical expressions we have derived, a semianalytical model of charge density, capacitance, and total energy (grand potential) is constructed.

The counterion Boltzmann equation in Eq. (9) provides a means of identifying the region of validity of the semianalytical approximation. The surface volume fraction φ_0 increases as surface potential Φ_0 increases. Formally φ_0 may never exceed 1, but the Carnahan–Starling potential is infinite at this limit. A more practical limit can be obtained treating the counterion as a hard sphere, such that φ_0 may not exceed the close packing limit [20], $\varphi_{max} = 0.74$ (i.e. $\pi/3\sqrt{2}$). For typical ions with radius 1–10 Å φ_{max} is reached at the surface when the surface potential exceeds 3–4 V. The semianalytical approximation may be considered valid up to this limit.

3.1. Semianalytical electrode charge density and capacitance

The electrode charge density σ can be calculated from the electric field at the electrode interface, $\sigma = \varepsilon E(x = 0)$, giving

$$\sigma = \mathrm{sgn}(\Phi_0)\sqrt{\frac{-6\varepsilon\Phi_0}{4}\frac{ze(c_0 + c_b)^2}{c_0 + 2c_b}} \tag{10}$$

An analytical expression for the differential capacitance $C = d\sigma/d\Phi_0$ can then be determined. This requires evaluation of the derivatives with respect to surface potential, $dH/d\Phi_0$ and $dc_0/d\Phi_0$, which are outlined in Supplementary Information. The resulting capacitance is

$$C = \frac{3\varepsilon}{2H}\left[\frac{c_0 + c_b}{c_0 + 2c_b} + \frac{c_0 + 3c_b}{(c_0 + 2c_b)^2}\frac{\beta z e c_0 \Phi_0}{\left(\varphi_0 \frac{2\varphi_0 - 8}{(1-\varphi_0)^4} - 1\right)}\right] \tag{11}$$

3.2. Grand potentials

The total grand potential (and therefore stored energy) of the electric double layer is composed of the ideal ion configuration entropy, electrostatic energy, and steric potential. We note that the energy is a grand potential rather than a free energy since ion adsorption proceeds relative to a bulk electrolyte with a constant bulk concentration that maintains a constant chemical potential for each ion. The entropic component is given by [21,22]

$$\Omega_{en} = k_B T \sum_i \int dx \left[c_i(x)\ln\frac{c_i(x)}{c_{ib}} - c_i(x) + c_{ib}\right] \tag{12}$$

The electrostatic component is given by

$$\Omega_{el} = \frac{\varepsilon_0 \varepsilon_s}{2}\int |E(x)|^2\, dx \tag{13}$$

For the steric component, we apply a thermodynamic integration, noting that simple summation of the steric potential [11] is not sufficient when the potential depends on ion concentrations. That is,

$$\Omega_{st} = \sum_i \int dx \int_{\lambda=0}^{\lambda=1} \Delta\mu_i^{st}(\lambda\varphi)\lambda c_i d\lambda \tag{14}$$

For the Carnahan–Starling steric potential, this evaluates to [23]

$$\Omega_{st} = k_B T \sum_i \int c_i \left[\frac{4\varphi - 3\varphi^2}{(1-\varphi)^2} - \frac{4\varphi_b - 3\varphi_b^2}{(1-\varphi_b)^2}\right] dx \tag{15}$$

The total grand potential Ω is the sum of the components, $\Omega = \Omega_{en} + \Omega_{el} + \Omega_{st}$.

Under the model of a linear steric layer with thickness H, the grand potential components reduce to semianalytical approximations,

$$\frac{\Omega_{en}}{k_B T} = \frac{H}{2}\left[\frac{c_0^2}{c_0 - c_b}\ln\left(\frac{c_0}{c_b}\right) + \frac{c_b - 3c_0}{2}\right] \tag{16}$$

$$\Omega_{el} = \frac{z^2 e^2 H^3}{120\varepsilon}\left[3c_0^2 + 9c_0 c_b + 8c_b^2\right] \tag{17}$$

and

$$\frac{\Omega_{st}}{k_B T} = \frac{H}{v}\left[\frac{1+3(1-\varphi_0)(1-\varphi_b)}{(1-\varphi_0)(1-\varphi_b)} + \frac{2}{(\varphi_b-\varphi_0)}\ln\left(\frac{1-\varphi_0}{1-\varphi_b}\right)\right] - \frac{H}{2}(c_b - c_0)\left[\frac{4-3\varphi_b}{(1-\varphi_b)^2}\right] \tag{18}$$

Note that all these parameters, namely the charge density, differential capacitance, and the grand potentials, are ion-size specific either directly through the ion volume v in their respective expressions or through the counterion concentration $c_0 = \varphi_0/v$.

4. Results and discussion

In this section, the results of the semianalytical model are presented. Initially, a comparison is made between the semianalytical model and full numerical solutions by examining the charge density profiles and differential capacitance over a range of electrode potentials and concentrations. The semianalytical model for grand potentials are also compared against their full numerical counterpart. Finally, the model is validated against experimental measurements of the differential capacitance for an aqueous NaF solution and molecular dynamics (MD) simulations of an ionic liquid of 1-ethyl-3-methylimidazolium bis(trifluoromethylsulfonyl)imide (EMIM−TFSI).

4.1. Comparison of semianalytical and full numerical solutions

A benchmark was first conducted by comparing the semianalytical model with full numerical solutions. We consider a salt solution of $LiPF_6$ which is commonly used in energy storage applications dissolved in propylene carbonate solvent. Hydrated-lithium ion of radius 2.82 Å and PF_6^- ion of radius 2.54 Å were used for modelling. We note that the dielectric constant of the solvent is concentration/electric field dependent in the solution and the effective value is less than the static dielectric constant [24]. However, for the first part of the analysis, we restrict ourselves to a uniform relative dielectric constant value of $\varepsilon_s = 66.14$ for propylene carbonate. We conducted a full numerical solution of the coupled equations given by Eqs. (2) and (3) with the CS steric potential, using Finite Element Methods implemented in FEniCS [25]. We calculated electrode potentials running from −1 V to 1 V and bulk ion concentrations of 0.01M, 0.1M, and 1M.

The full numerical differential capacitance is then calculated through the electrode charge density as $C = (\sigma(\Phi_0 + \Delta\phi) - \sigma(\Phi_0))/\Delta\phi$ with $\Delta\phi = 0.01$ mV. The full numerical grand potentials are also computed by integrating the electrostatic potentials and ions concentration obtained numerically, using Eqs. (12)–(14).

Calculated counterion concentrations and the corresponding electric field are shown in Fig. 2, comparing 0.01M, 0.1M, and 1M bulk concentrations with electrode potential 0.9 V. Counterion concentrations from the full numerical solution, Fig. 2(a)–(c), indicate that the model of a linearly falling counterion concentration (Eq. (4)) improves as the bulk concentration increases. The working electrode potential of common electric double-layer capacitors is 2.5–2.7 V, with electrolyte

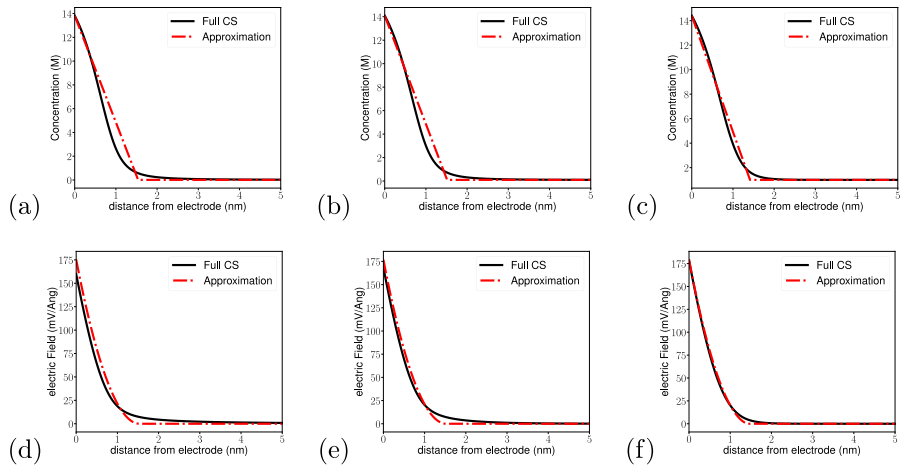

Fig. 2. Comparison of the full numerical solution with the semianalytical approximation of (a)–(c) the counterion concentration profile (d)–(f) the electric field at potential 1 V for bulk concentrations of 0.01M, 0.1M and 1M, respectively.

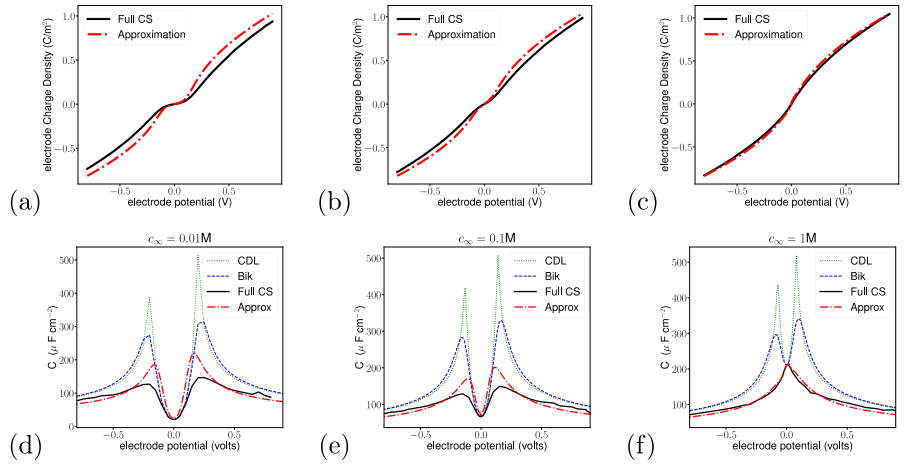

Fig. 3. Comparison of the full numerical solution with the semianalytical approximation for (a)–(c) the electrode charge density (d)–(f) the differential capacitance for bulk concentrations of 0.01M, 0.1M, and 1M. For comparison, we also include capacitance from CDL and Bikerman models.

concentration exceeding 1M, justifying the approximation of linear counterion decay. The semianalytical electric field approximations in Fig. 2(d)–(f) (likewise the electrostatic potentials) also match the full numerical curve with increasing accuracy at high potential and high concentration.

Calculated surface charge densities and electrode capacitances are shown in Fig. 3 as a function of electrode potential. The semianalytical expressions for these quantities reproduce the full numerical solutions well, particularly at high concentration and voltage, reaching a relative error of <2% at ~1 V and bulk concentration of 1M. The capacitance in Fig. 3(d)–(f) also shows a transition from the camel to bell shape at high density, matching the full numerical results with relative error <5% at 1 V and concentration 1M.

4.2. Grand potentials

Calculated grand potentials are presented in Fig. 4, showing the relative contributions of each component. The ion entropic component (Eq. (12)) is significant at low potentials and low concentration, but diminishes in importance as the electrode potential increases, as seen in Fig. 4(a).

Fig. 4(b) shows an asymptotic trend, with the steric contribution to the grand potential accounting for approximately one quarter of the total energy at high electrode potentials, while the contribution of ideal ion entropy becomes largely insignificant. This trend is consistent with that seen in the simpler CDL, where the steric contribution comprised half of the total energy [11]. That is, as the electrode potential rises, increasing the electrostatic energy, the steric energy rises proportionally, similar to the steric push-back mechanism used to construct CDL models.

The error in the semianalytical approximation for the total grand potential relative to the full numerical calculation is shown in Fig. 4(c). At low electrolyte concentration and lower electrode potential, the error is quite large. This higher error in these regimes is attributed to the limitation of the analytical model, with the counterion concentration following a conventional exponential decay rather than linear decay when the electrode potential lies below the critical steric potential (<0.2 V). Nevertheless, the error diminishes as electrode potential increases. At 1M concentrations the error is less than 5% once the potential exceeds 0.2 V.

4.3. Validation against literature

To further test the validity of the semianalytical model for differential capacitance, we compare it against results from literature, firstly experimental data for silver electrodes in 0.1M NaF aqueous solution [26], and then molecular dynamics simulations of an ionic liquid [27].

In both examples, the dielectric constant in the steric layer is determined as an average effective permittivity ε_{eff} that accounts for

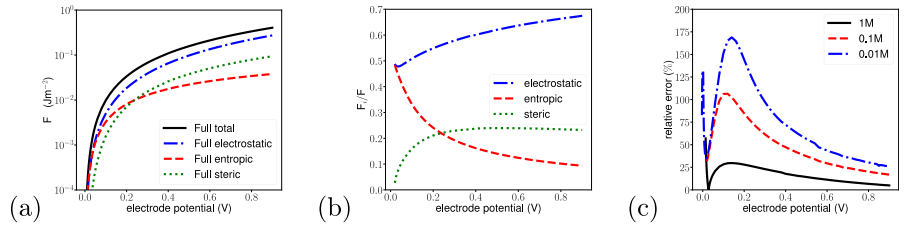

Fig. 4. (a) Energy (grand potential) components at a bulk concentration of 1M. (b) The fraction of the components of the grand potential relative to the total at a bulk density of 1M. (c) relative error of the semianalytical grand potential approximation to the full numerical solution for the bulk densities of 0.01M, and 1M.

the size and permittivity ε_i of the adsorbed counterion in the layer. The average permittivity is determined via the Garnett mixing variant of the Clausius–Mossotti equation [28],

$$\frac{\varepsilon_{\text{eff}} - \varepsilon_s}{\varepsilon_{\text{eff}} + 2\varepsilon_s} = \frac{\varepsilon_i - \varepsilon_s}{\varepsilon_i + 2\varepsilon_s}\varphi_0,$$

where φ_0 is the counterion volume fraction at the surface, determined by resolving Eq. (9) for a given surface potential. ε_s is the dielectric constant of the medium.

The permittivity ε_i of each ion is related to its polarizability α_i, treating the ion as a dielectric sphere with volume υ_i [29],

$$\frac{\varepsilon_i - 1}{\varepsilon_i + 2} = \frac{4\pi}{3\upsilon_i}\alpha_i \tag{19}$$

where both υ_i and α_i are in volume units (Å^3). Our two examples illustrate different methods for determining the relevant input parameters ε_s, α_i and υ_i from literature. But in both cases we find that consideration must be given to dielectric saturation in the steric layer, reducing the magnitude of ε_{eff}.

4.3.1. Aqueous NaF (experimental data)

Valette conducted extensive measurements of the differential capacitance of various silver crystal surfaces [26,30–32]. For the purpose of testing the success of the semianalytical approximation, we consider the case of 0.1M NaF measured at the 111 crystal face [26], considered also in a recent paper on the Stern layer [33]. We apply the semianalytical approximation comparing two alternative sets of ion volumes. Firstly we consider Marcus' hydrated ion radii [34], with $r_{\text{Na}} = 2.18$Å and $r_{\text{F}} = 2.12$ Å. The second set represents the hydrated radius of Na with a larger value given by the average distance from the ion to the hydrogen atom of water molecules in the hydration shell, $r_{\text{MH}} = 2.93$ Å, determined from radial distribution functions obtained by Ohtaki *et al* by computer simulations [35]. For F$^-$, the hydrated radius was reduced slightly to 1.95Å to better fit the experimental capacitance at positive voltages. In both cases the polarizabilities of the hydrated ions were estimated by adding the polarizability of the bare ion to the polarizability of tightly bound water molecules. The electronic polarizability of the bare ions, previously calculated by quantum chemical methods [36], were given by $\alpha_{\text{Na}} = 0.139$ Å^3 and $\alpha_{\text{F}} = 1.913$ Å^3, and $\alpha_{\text{water}} = 1.4255$ Å^3 for a single water molecule is given by [37]. The average numbers of water molecules in the hydration shells were given by Marcus' hydration numbers, 3.5 and 2.7 for Na$^+$ and F$^-$, respectively [34]. We found that using the bulk permittivity of water (78.4), capacitances are vastly over estimated. Instead, it is appropriate to use a reduced solvent permittivity that accounts for dielectric saturation. We therefore applied a surface water permittivity $\varepsilon_s = 7.19$, following Devanathan and Tilak [38].

The differential capacitance of the aqueous NaF solution is plotted in Fig. 5 as a function of electrode potential. The black dashed line corresponds to the experimental data, and the red (dash-dotted) and blue (solid) curves represent the values from the semianalytical model using Marcus hydrated ion radii, and Ohtaki's r_{MH} hydrated radii, respectively.

The overall experimental trend is reproduced by both semianalytical curves, with the right general magnitude obtained by applying a reduced solvent permittivity that accounts for dielectric saturation. The curve obtained by Marcus radii captures the camel-shaped capacitance profile, however, it shows noticeable deviations. The Na$^+$ radius appears to be underestimated, leading to an exaggerated differential capacitance at large negative potentials, while the F$^-$ radius seems to be overestimated, resulting in lower capacitance values at positive potentials. In contrast, the values from the larger r_{MH} radius for Na$^+$, and reduced fitted radius for F$^-$, exhibit excellent agreement with the experimental data, particularly in the extreme potential regimes. The peak positions and magnitudes are more accurately captured when the r_{MH} radii are used, suggesting that these radii provide a more suitable representation of the effective ion sizes in the aqueous solutions. The sodium peak at negative potentials is in excellent agreement with the experimental result, capturing both the magnitude and location of the peak. The F$^-$ peak at positive potential overestimates the magnitude of the peak, but still captures the location of the peak and follows the experimental data well at higher potentials. Curiously, a similar theoretical curve can be obtained using Ohtaki's radius $r_{\text{MH}} = 1.6$ Å for F$^-$, if the polarizability of hydration waters is not added to the F$^-$ polarizability. This raises the question of whether the hydration shell of F$^-$ is partially removed or weakened by adsorption in the steric layer, which would be consistent with the observation of specific adsorption of F$^-$ that Valette reported on this silver electrode.

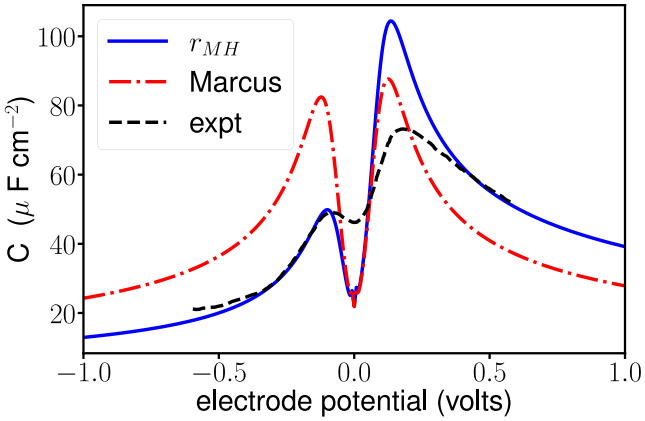

Fig. 5. Differential capacitance of an aqueous 0.1M NaF solution as a function of electrode potential. Black dashed line: experimental data [26]; red dash-dotted: semianalytical model with Marcus hydration radii [34]; blue solid curves: with radius r_{MH} 2.93 Å for Na$^+$ and reduced hydration radius 1.95 Å for F$^-$.

4.4. Ionic liquid EMIM−TFSI (molecular dynamics data)

In this application, we aim to demonstrate how successfully the semianalytical approximation can describe a complex ionic liquid under conditions of relative ignorance of ion size, estimating the concentration from the bulk mass density and molar mass of the ionic liquid, fitting only the ion polarizabilities. We compare the semianalytical approximation against the simulated capacitance of a graphite electrode in a room temperature ionic liquid EMIM−TFSI, with molecular

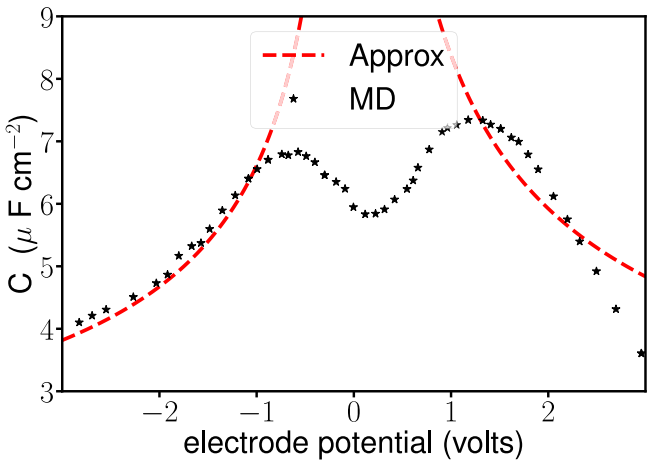

Fig. 6. Differential capacitance of EMIM−TFSI ionic liquid as a function of electrode potential. The red dashed lines shows the theoretical approximation using the effective dielectric function while black stars indicate molecular dynamics simulation data from Ref. [27]. An equivalent of bulk concentration of 3.89M was calculated from mass density 1522 kg/m^3 and molar mass 391.31 g/mol of the ionic liquid.

dynamics simulations computed by Vatamanu et al. [27] The MD simulations employed nonpolarizable explicit atom/united atom (EA/UA) hybrid force fields. Vatamanu found more irregular capacitance profiles with geometrically flat surfaces, attributed to specific adsorption of alkyl chains, that tend to lie flat on the smooth surface. We therefore compare against the MD results for EMIM-TSFI on "rough" surfaces.

For this system, ionic radii were estimated from the mass density 1522 kg/m^3 and molar mass 391.31 g/mol of the ionic liquid EMIM−TFSI [27]. The average ion radius is 3.7 Å, applied to both cation and anion, is consistent with reported EMIM$^+$ and TFSI$^-$ dimensions [39]. The corresponding bulk concentration is 3.89 M. The average ion polarizability determined via Eq. (19) from the bulk permittivity $\varepsilon = 12$ and the average volume per ion would be 40 Å^3. As in the aqueous case above, we employ a smaller polarizability in the steric adsorption layer to account for dielectric saturation, removing the rotational polarizability of the ions. In lieu of estimating the permanent dipoles and corresponding rotational polarisabilites, we simply fit the remaining (electronic) polarizabilities to match the MD data. The ion polarizabilities are taken as 8 Å^3 for EMIM$^+$ and 17 Å^3 for TFSI$^-$, to give an ion permittivity of 1.562 and 2.515 respectively. These were used within the Clausius–Mossotti (Garnett) framework, Eq. (19), to calculate the dielectric constant in the adsorption layer, with $\varepsilon_s = 1$ since the ionic liquid has no solvent.

The differential capacitance estimated by the semianalytical approximation is shown in Fig. 6. The semianalytical approximation (red dashed line) converges to the MD simulation results (black stars) in high potential regimes ($|V| > 1$ V).

We find that the semianalytical approximation, while reasonable or even good at high potentials, shows significant deviation from the MD results in the low potential regime. The high potential regime beyond the peaks is the region where the steric forces represented by the semianalytical model are significant, and the success of the model in this region indicates that the behaviour at high potentials is dominated by the steric forces. The behaviour of the model at low potentials was nevertheless reasonable in the case of the aqueous system above, Fig. 5, while completely failing to describe the ionic liquid well at low potentials below the steric peak. The Carnahan–Starling model used to describe the steric forces is designed to reproduce the equation of state of a liquid to the 10th virial coefficient [15], thereby describing many-body hard-sphere interactions of the liquid well. That is, the Carnhan–Starling model, represented by the semianalytical approximation, can be understood as representing ion-ion hard sphere correlations within the framework of a continuum model of the electrolyte. What is missing from the theory are electrostatic correlations. Electrostatic correlations are relatively weak in aqueous electrolytes, at least with monovalent ions and at concentrations below 1M. But in ionic liquids they are indispensible [40], at least in the low potential region before steric hard sphere correlations begin to dominate. We tentatively attribute the failure to describe the capacitance of the ionic liquid at low potentials to the lack of electrostatic correlations in mean-field continuum theory.

We note that at large negative potentials, where the semianalytical approximation describes the MD results well, the capacitance curves are concave up with respect to potential. The same is true for the aqueous capacitance in Fig. 5. At high positive potentials, however, the MD data shows a linear profile not matching the semianalytical approximation, which remains concave up. We take this quality to be a marker indicating whether the semianalytical approximation can be applied successfully. The absence of a concave-up capacitance profile may indicate insufficient sampling in computer simulations, or the presence of other phenomena such as redox reactions in experimental systems. The analytical approximation has a bell-shaped profile with a peak at zero potential that would reach 87 μF/cm^2, where the MD results show a camel-shaped capacitance profile with a peak of only 7 μF/cm^2 near 1 V. However, the higher potential regions where the semianalytical approximation is successful cover voltages relevant to applications such as energy storage.

5. Conclusion

We have presented a semianalytical approximation of the Equation-of-State models of steric force, exemplified by the Carnahan–Starling model of an electric double-layer capacitor. Our approximation is based on the linear counterion concentration profile observed in exact CS calculations, valid for surface potentials in the range 0.2–4 V. We have shown that these approximations agree well with the full numerical solution of the CS equations in the limit of high potential and electrolyte concentration with relative error less than 2% for the surface charge density, and less than 5% for the differential capacitance and the total grand potential. The relative error reduces as electrode potential or electrolyte concentration increases, justifying the use of the approximations for modelling supercapacitors where the working potential and electrolyte concentration are high. Once dielectric saturation is accounted for, reducing the permittivity in the steric adsorption layer, semianalytical capacitance calculations are in good agreement with literature values, both experimental and computer simulation, particularly in high potential regimes. The model may be applied to ionic liquids at high potentials, though not at low potentials <1 V. Our analytical approximations immensely simplify the computation time and effort needed to solve a highly nonlinear differential equation without compromising the accuracy of the solution. The results demonstrate that the semianalytical approach is capable of reproducing the differential capacitances, especially at electrochemically relevant potentials.

CRediT authorship contribution statement

Dagmawi B. Tadesse: Writing – original draft, Software, Methodology, Investigation, Formal analysis, Conceptualization. **Drew F. Parsons:** Writing – review & editing, Supervision, Software, Resources, Methodology, Conceptualization.

Declaration of competing interest

The authors declare that they have no known competing financial interests or personal relationships that could have appeared to influence the work reported in this paper.

Acknowledgements

The authors would like to acknowledge computational support from the West Australian Pawsey Supercomputing Centre. We also acknowledge the award of CINECA support under the Italian ISCRA initiative, for the availability of high-performance computing resources and support.

D.F.P conceptualized the work and edited the text; D.B.T derived mathematical approximations, conducted calculations and prepared original text and figures. Both authors contributed equally to software writing.

Appendix A. Supplementary data

Supplementary material related to this article can be found online at https://doi.org/10.1016/j.electacta.2025.146266.

Data availability

Data will be made available on request.

References

[1] J.J. Bikerman, Structure and capacity of electrical double layer, Lond. Edinb. Dublin Philos. Mag. J. Sci. 33 (220) (1942) 384–397, http://dx.doi.org/10.1080/14786444208520813.
[2] M. Eigen, E. Wicke, The thermodynamics of electrolytes at higher concentration, J. Phys. Chem. 58 (9) (1954) 702–714, http://dx.doi.org/10.1021/j150519a007.
[3] N.F. Carnahan, K.E. Starling, Equation of state for nonattracting rigid spheres, J. Chem. Phys. 51 (2) (1969) 635–636, http://dx.doi.org/10.1063/1.1672048.
[4] T. Boublík, Hard-sphere equation of state, J. Chem. Phys. 53 (1) (1970) 471–472, http://dx.doi.org/10.1063/1.1673824.
[5] G.A. Mansoori, N.F. Carnahan, K.E. Starling, T.W. Leland, Equilibrium thermodynamic properties of the mixture of hard spheres, J. Chem. Phys. 54 (4) (1971) 1523–1525, http://dx.doi.org/10.1063/1.1675048.
[6] I. Borukhov, D. Andelman, H. Orland, Steric effects in electrolytes: A modified Poisson-Boltzmann equation, Phys. Rev. Lett. 79 (3) (1997) 435–438, http://dx.doi.org/10.1103/PhysRevLett.79.435.
[7] M.S. Kilic, M.Z. Bazant, A. Ajdari, Steric effects in the dynamics of electrolytes at large applied voltages. I. Double-layer charging, Phys. Rev. E 75 (2) (2007) 21502, http://dx.doi.org/10.1103/PhysRevE.75.021502.
[8] A.A. Kornyshev, Double-layer in ionic liquids: Paradigm change? J. Phys. Chem. B 111 (20) (2007) 5545–5557, http://dx.doi.org/10.1021/jp067857o.
[9] J.M. Borah, S. Mahiuddin, N. Sarma, D.F. Parsons, B.W. Ninham, Specific ion effects on adsorption at the solid/electrolyte interface: A probe into the concentration limit, Langmuir 27 (14) (2011) 8710–8717, http://dx.doi.org/10.1021/la2006277.
[10] D.F. Parsons, The impact of nonelectrostatic physisorption of ions on free energies and forces between redox electrodes: ion-specific repulsive peaks, Electrochim. Acta 189 (2016) 137–146, http://dx.doi.org/10.1016/j.electacta.2015.12.090.
[11] D.B. Tadesse, D.F. Parsons, The impact of steric repulsion on the total free energy of electric double layer capacitors, Colloids Surf. A: Physicochem. Eng. Asp. 648 (2022) 129134, http://dx.doi.org/10.1016/j.colsurfa.2022.129134.
[12] M.Z. Bazant, M.S. Kilic, B.D. Storey, A. Ajdari, Towards an understanding of induced-charge electrokinetics at large applied voltages in concentrated solutions, Adv. Colloid Interface Sci. 152 (1) (2009) 48–88, http://dx.doi.org/10.1016/j.cis.2009.10.001.
[13] J. López-García, J. Horno, C. Grosse, Differential capacitance of the diffuse double layer at electrode-electrolyte interfaces considering ions as dielectric spheres: Part I. Binary electrolyte solutions, J. Colloid Interface Sci. 496 (2017) 531–539, http://dx.doi.org/10.1016/j.jcis.2017.02.043.
[14] A. Mulero, C.A. Faúndez, F. Cuadros, Chemical potential for simple fluids from equations of state, Mol. Phys. 97 (1999) 453–462, http://dx.doi.org/10.1080/00268979909482845.
[15] A. Santos, Chemical-potential route: A hidden Percus-Yevick equation of state for hard spheres, Phys. Rev. Lett. 109 (2012) 120601, http://dx.doi.org/10.1103/PhysRevLett.109.120601.
[16] H. Liu, Carnahan-Starling type equations of state for stable hard disk and hard sphere fluids, Mol. Phys. 119 (9) (2021) e1886364, http://dx.doi.org/10.1080/00268976.2021.1886364.
[17] B. Giera, N. Henson, E.M. Kober, M.S. Shell, T.M. Squires, Electric double-layer structure in primitive model electrolytes: Comparing molecular dynamics with local-density approximations, Langmuir 31 (11) (2015) 3553–3562, http://dx.doi.org/10.1021/la5048936, PMID: 25723189.
[18] G.V. Bossa, D.L.Z. Caetano, S.J. de Carvalho, K. Bohinc, S. May, Modeling the camel-to-bell shape transition of the differential capacitance using mean-field theory and Monte Carlo simulations, Eur. Phys. J. E 41 (9) (2018) 113, http://dx.doi.org/10.1140/epje/i2018-11723-7.
[19] W. Dou, M. Chen, S. Zhou, Fast iterative method for local steric Poisson–Boltzmann theories in biomolecular solvation, Comput. Phys. Comm. 291 (2023) 108808, http://dx.doi.org/10.1016/j.cpc.2023.108808.
[20] S. Neser, C. Bechinger, P. Leiderer, T. Palberg, Finite-size effects on the closest packing of hard spheres, Phys. Rev. Lett. 79 (1997) 2348–2351, http://dx.doi.org/10.1103/PhysRevLett.79.2348.
[21] C.G. Gray, P.J. Stiles, Nonlinear electrostatics: the Poisson–Boltzmann equation, Eur. J. Phys. 39 (2018) 053002, http://dx.doi.org/10.1088/1361-6404/aaca5a.
[22] D. Tadesse, D.F. Parsons, Thermodynamics beyond dilute solution theory: Steric effects and electrowetting, in: Encyclopedia of Solid-Liquid Interfaces, Vol. 1–3, Elsevier, 2024, pp. 126–135, http://dx.doi.org/10.1016/B978-0-323-85669-0.00137-9.
[23] D. Antypov, M.C. Barbosa, C. Holm, Incorporation of excluded-volume correlations into Poisson-Boltzmann theory, Phys. Rev. E 71 (2005) 061106, http://dx.doi.org/10.1103/PhysRevE.71.061106.
[24] L. Yang, B.H. Fishbine, A. Migliori, L.R. Pratt, Dielectric saturation of liquid propylene carbonate in electrical energy storage applications, J. Chem. Phys. 132 (4) (2010) 044701, http://dx.doi.org/10.1063/1.3294560.
[25] M.S. Alnæs, J. Blechta, J. Hake, A. Johansson, B. Kehlet, A. Logg, C. Richardson, J. Ring, M.E. Rognes, G.N. Wells, The FEniCS project version 1.5, Arch. Numer. Softw. 3 (100) (2015) http://dx.doi.org/10.11588/ans.2015.100.20553.
[26] G. Valette, Double layer on silver single crystal electrodes in contact with electrolytes having anions which are slightly specifically adsorbed: Part III. The (111) face, J. Electroanal. Chem. Interfacial Electrochem. 269 (1) (1989) 191–203, http://dx.doi.org/10.1016/0022-0728(89)80112-3.
[27] J. Vatamanu, O. Borodin, D. Bedrov, G.D. Smith, Molecular dynamics simulation study of the interfacial structure and differential capacitance of alkylimidazolium bis(trifluoromethanesulfonyl)imide [Cnmim][TFSI] ionic liquids at graphite electrodes, J. Phys. Chem. C 116 (14) (2012) 7940–7951, http://dx.doi.org/10.1021/jp301399b.
[28] T.C. Choy, Effective Medium Theory: Principles and Applications, Oxford University Press, 2015, http://dx.doi.org/10.1093/acprof:oso/9780198705093.001.0001.
[29] J. Fiedler, P. Thiyam, A. Kurumbail, F.A. Burger, M. Walter, C. Persson, I. Brevik, D.F. Parsons, M. Boström, S.Y. Buhmann, Effective polarizability models, J. Phys. Chem. A 121 (51) (2017) 9742–9751, http://dx.doi.org/10.1021/acs.jpca.7b10159, PMID: 29185741.
[30] G. Valette, A. Hamelin, Structure et propriétés de la couche double électrochimique à l'interphase argent/solutions aqueuses de fluorure de sodium, J. Electroanal. Chem. Interfacial Electrochem. 45 (1973) 301–319, http://dx.doi.org/10.1016/S0022-0728(73)80166-4.
[31] G. Valette, Double layer on silver single-crystal electrodes in contact with electrolytes having anions which present a slight specific adsorption, J. Electroanal. Chem. Interfacial Electrochem. 122 (1981) 285–297, http://dx.doi.org/10.1016/S0022-0728(81)80159-3.
[32] G. Valette, Double layer on silver single crystal electrodes in contact with electrolytes having anions which are slightly specifically adsorbed: Part II. the (100) face, J. Electroanal. Chem. Interfacial Electrochem. 138 (1) (1982) 37–54, http://dx.doi.org/10.1016/0022-0728(82)87126-X.
[33] X. Wang, K. Liu, J. Wu, Demystifying the stern layer at a metal–electrolyte interface: Local dielectric constant, specific ion adsorption, and partial charge transfer, J. Chem. Phys. 154 (12) (2021) 124701, http://dx.doi.org/10.1063/5.0043963.
[34] Y. Marcus, Thermodynamics of solvation of ions. Part 5.—Gibbs free energy of hydration at 298.15 K, J. Chem. Soc. Faraday Trans. 87 (1991) 2995–2999, http://dx.doi.org/10.1039/FT9918702995.
[35] H. Ohtaki, T. Radnai, Structure and dynamics of hydrated ions, Chem. Rev. 93 (3) (1993) 1157–1204, http://dx.doi.org/10.1021/cr00019a014.
[36] D.F. Parsons, B.W. Ninham, Importance of accurate dynamic polarizabilities for the ionic dispersion interactions of alkali halides, Langmuir 26 (3) (2010) 1816–1823, http://dx.doi.org/10.1021/la902533x, PMID: 20099919.
[37] D.F. Parsons, B.W. Ninham, Charge reversal of surfaces in divalent electrolytes: The role of ionic dispersion interactions, Langmuir 26 (9) (2010) 6430–6436, http://dx.doi.org/10.1021/la9041265, PMID: 20112936.
[38] M.A.V. Devanathan, B.V.K.S.R.A. Tilak, The structure of the electrical double layer at the metal-solution interface, Chem. Rev. 65 (1965) 635–684, http://dx.doi.org/10.1021/cr60238a002.
[39] A. Elbourne, S. McDonald, K. Voïchovsky, F. Endres, G.G. Warr, R. Atkin, Nanostructure of the ionic liquid–graphite stern layer, ACS Nano 9 (7) (2015) 7608–7620, http://dx.doi.org/10.1021/acsnano.5b02921, PMID: 26051040.
[40] R. Kjellander, Nonlocal electrostatics in ionic liquids: The key to an understanding of the screening decay length and screened interactions, J. Chem. Phys. 145 (2016) http://dx.doi.org/10.1063/1.4962756.